Supporting Information

Vacancy-Modified Few-layered GaN Crystal for Novel High-Temperature Energy Storage

Songyang Lv[a], Shouzhi Wang[,a], Tailin Wang[b], Lei Liu[a], Jiaoxian Yu[b], Tianran Dong[a] Guodong Wang[*,a], Zhongxin Wang[a], Chang Liang[a], Lili Li[*,c], Xiangang Xu[a], Lei Zhang[*,a]*

[a]Institute of Novel Semiconductors, State Key Lab of Crystal Materials, Shandong University, Jinan, 250100, P. R. China.

[b]Key Laboratory of Processing and Testing Technology of Glass & Functional Ceramics of Shandong Province, School of Materials Science and Engineering, Qilu University of Technology (Shandong Academy of Sciences), Jinan 250353, P. R. China.

[c]Key Laboratory of Interfacial Physics and Technology, Shanghai Institute of Applied Physics, Chinese Academy of Sciences, Shanghai, 201800, P. R. China.

*E-mail: wangsz@sdu.edu.cn; guodong9631@sdu.edu.cn; lilili@sinap.ac.cn leizhang528@sdu.edu.cn.

This file includes:

S1. Materials

Reagents were purchased from Sinopharm Chemical Reagent Co., Ltd. (Shanghai). All the reagents were used as received.

S2. Theoretical calculation method

The present calculations were carried out by Vienna Ab initio Simulation Package (VASP) [1,2] implementation of DFT in conjunction with the projector augmented wave (PAW) formalism. Consequently, the H $1s^1$, C $2s^22p^2$, N $2s^22p^3$, O $2s^22p^4$, F $2s^22p^5$, S $3s^23p^4$, and Ga $4s^2$, $3d^{10}$, $4p^1$ states are treated as valence electrons. The electronic wave functions were expanded in plane waves using an energy cut off of 500 eV. The convergence criteria of force and energy for the structural relaxation were set at 0.01 eV/Å and 10^{-5} eV. The lattice parameters of primitive hexagonal GaN were a=b=3.19 Å, c=5.19 Å after optimization. Then constructed the 2 × 2× 2 supercells to model nitrogen vacancy defect (V_N@GaN), as shown in **Figure S16**. The electron exchange and correlation (XC) of the generalized gradient approximation (GGA) functional of Perdew, Burke, and Ernzerhof (PBE) were used to optimize the configurations[3]. All the electronic properties of GaN and V_N@GaN were determined using the screened Heyde-Scuseriae-Ernzerhof (HSE) hybrid functional[4,5]. In this approach, the long-range exchange potential and the correlation potential were calculated with the PBE functional, while the short-range exchange potential was calculated by mixing a fraction of the non-local Hartreee-Fock exchange with PBE. The screening length and mixing parameter were fixed at 10 Å and 0.25, respectively. Monkhorst-Pack *k*-points[6] were sampled using a 4 × 4× 4 for

the relaxation and total energy and electronic calculations.

Each adsorption model is allowed to interact with $C_6H_{11}N_2$•$C_2F_6NO_4S_2$ ($EMImNFT_2$) and the adsorption energy (E_{ad}) for species X is defined as follows:

$$E_{ad} = E\,(\text{surface/X}) - E\,(\text{surface}) - E\,(\text{X})$$

where E(surface/X) is the total energy of the fully relaxed surface/adsorbate system, E(surface) is the total energy of the relaxed substrate slab, and E(X) is the total energy of a free adsorbate species ($EMImNFT_2$). Negative adsorption energy means effective adsorbate binding.

S3. Characterization Methods

The morphology of the as-collected samples was characterized by investigated by SEM (Hitachi S-4800), TEM (Philips Tecnai 20U-Twin), HRTEM (JEM 2100F), AFM (Nanoscope MultiMode V, Digital Instruments Dimension 3100 system). The crystal structures were obtained by XRD (Bruker diffractometer D8 Advance, Cu Kα radiation, λ = 1.5418 Å), XPS (Thermo ESCALAB 250 Al Kα radiation, 1486.8 eV), BET (ASAP 2020 sorptometer), PSD (BJH desorption dV/dlog(r) plot volume), Raman (Horiba Jobin Yvon with Ar^+ laser 532 nm), PL (at room temperature using 325 nm He–Cd lasers as the excitation source), EPR (JEOL (FA200), at X-band (≈ 9 GHz) at 123.15 K).

To measurement the conductivity of the samples, GaN-2.5h samples were dispersed in ethanol by a sonication process. The mixture was then dropped onto Si substrate with a 300-nm-thick SiO_2 layer. Prior to the photolithography process, the SiO_2/Si substrate was cleaned by dilute hydrofluoric acid (HF), dilute hydrochloric

acid (HCl), ethanol and deionized water. A typical photolithography process was used to print electrodes on top of nanosheets.

Electrical contact to the GaN-2.5h samples were made by defining source-drain electrodes separated by ~1000 nm with lithography technology (SUSS MicroTec MBJ4) and subsequent evaporation of 50 nm Ti and 50 nm Au. Rapid thermal annealing was carried out at 500 °C for 3 min in the forming gas (10% H_2 in He) to improve the contact and passivate Si-SiO_x interface traps.1 The Ti/Au (30/50 nm) electrodes can maintain a good contact interface with nanosheet.

S4. Electrochemical Measurements.

Electrochemical performance tests were performed with the CHI660E electrochemical workstation. For the three-electrode test system with few-layer GaN crystal as the working electrode (The area of active material on the stainless-steel cloth was 1.5 cm^2, and the mass loading was about 1 mg cm^{-2}), a platinum plate as the counter electrode, Ag/AgCl as the reference electrode and in the electrolyte of 2M KCl solution. The CV and GCD curves were carried out in –0.3 V to 0.7 V under 25℃. In two-electrode measurements, the CV and GCD test data was collected at 0–2.7 V range from 25 ℃ to 150 ℃. The alternating current (AC) EIS spectrum was acquired range from 10^{-2} Hz to 10^5 Hz at an open circuit voltage with an AC amplitude of 0.005V. Mott-Schottky (M-S) for the measured frequency of 973Hz.

The area specific capacity of the electrodes in three-electrode test system, is derived from the GCD curve, calculated according to equation 1.

$$C = \frac{I\Delta t}{S\Delta V}$$

Where C is the specific capacitance (F cm^{-2}) base on the area of the electrode materials, I is the discharge current (A), Δt is the discharge time (s), S is the area (cm^2) of the active materials of the single electrode, ΔV is the working voltage window (V).

The area specific capacitance for IL-based SC device is calculated from equation 2

$$C = \frac{I\Delta t}{S\Delta V}$$

Where C is the area specific capacitance (F cm^{-2}) of the IL-based SC device, I is the discharge current (A), Δt is the discharge time (s), S is the total area (cm^2) of active material on the IL-based SC device, ΔV is the working voltage window (V).

The energy density of the IL-based SC device is calculated by equation 3

$$E = \frac{1}{2} C\Delta V^2$$

Where E is the energy density (mWh cm^{-2}) of the device, C is the area specific capacitance (mF cm^{-2}) of IL-based SC device, ΔV is the working voltage window (V).

The power density of the IL-based SC device is calculated by equation 4

$$P = \frac{E}{\Delta t}$$

Where P is the power density (mW cm^{-2}) of the device, E is the energy density (mWh cm^{-2}), Δt is the discharge time (s).

According to the M-S theory, the calculated electron concentration, was derived from equation 5

$$\frac{1}{C_s^2} = \frac{2}{(\varepsilon\varepsilon_0 e_0 N_d)}(U - U_{fb} - \frac{\kappa_B T}{e_0})$$

Where C_s is the space charge capacitance per unit area (F cm^{-2}), N_d is the electron concentration (cm^{-3}), ε is the dielectric constant, ε_0 is the permittivity of vacuum (F m^{-1}), e_0 is the electron charge (C), U is the applied potential (V), U_{fb} is the flat band potential (V), T is the temperature (K), and κ_B is the Boltzmann constant (J K^{-1}).

S5. Calculation of Capacitance Contribution

Equation 6

$$i(V) = k_1 v + k_2 v^{\frac{1}{2}}$$

We are interested in the percentage of the capacitive current.

S6. Supplementary Figures S1-S20

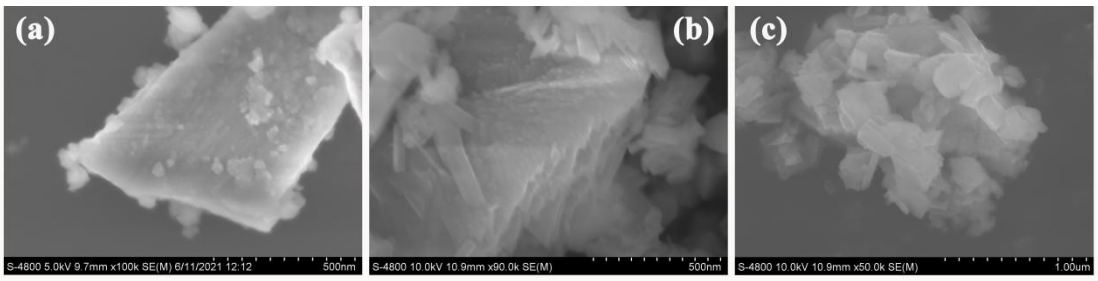

Figure S1. The SEM image of GaN crystal under different preparation time. GaN-1h (a); GaN-2.5h (b) and GaN-3h (c).

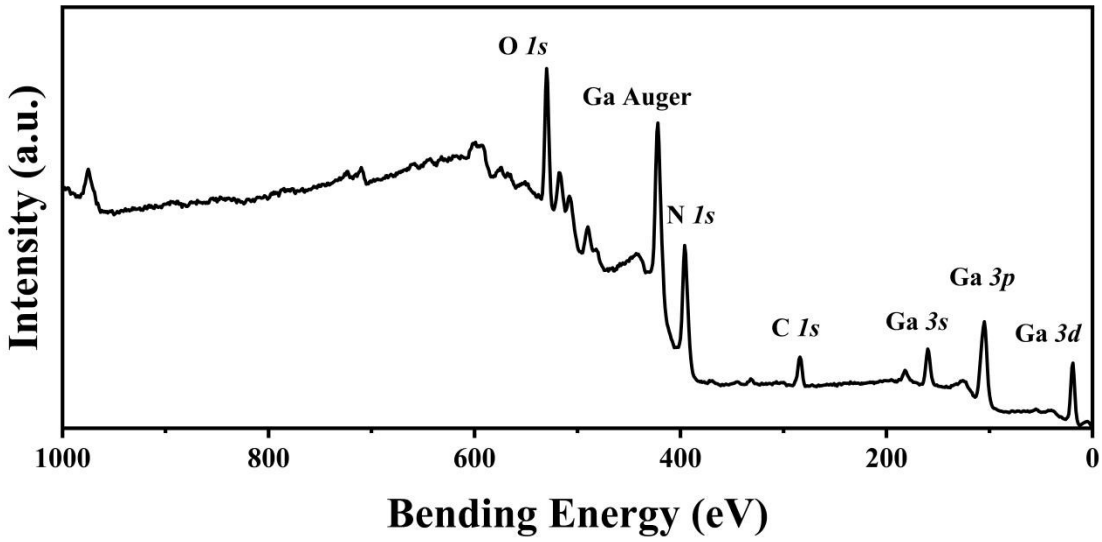

Figure S2. The XPS survey of few-layered GaN-2.5h crystal.

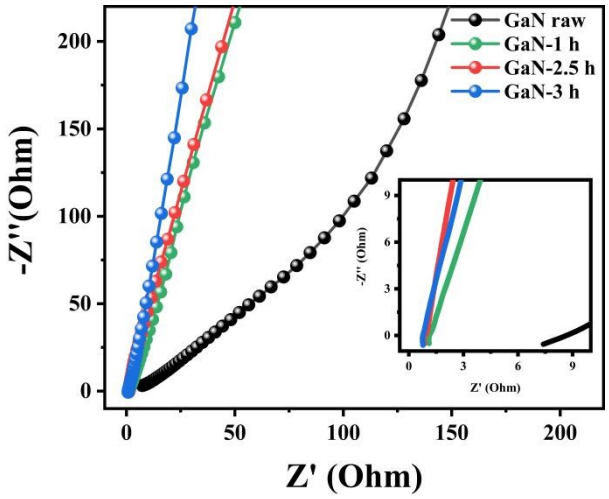

Figure S3. Three-electrode EIS tests. Nyquist plots of GaN raw, GaN-1h, GaN-2.5h and GaN-3h electrode.

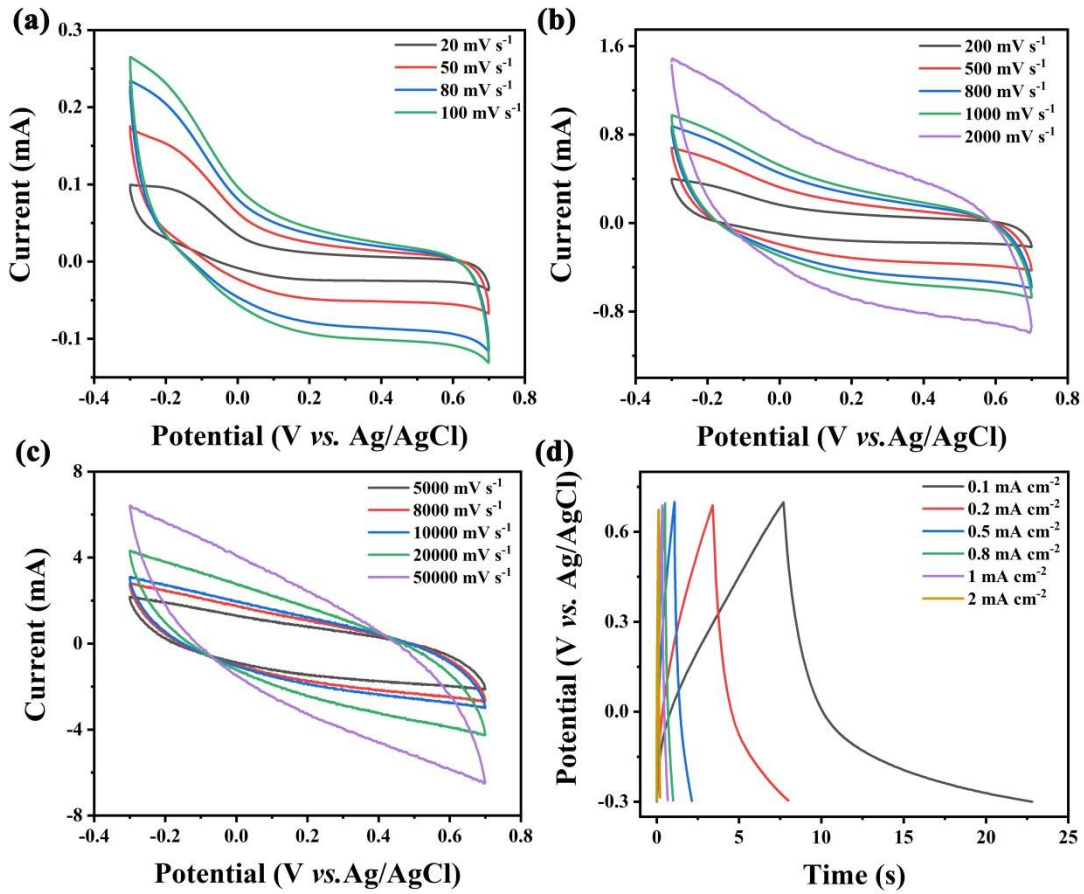

Figure S4. Three-electrode electrochemical performance of GaN raw. CV profiles of the electrode at scan rates ranging from 20 mV s^{-1} to 100 mV s^{-1} (a); from 200 mV s^{-1} to 2,000 mV s^{-1} (b) and from 5,000 mV s^{-1} to 50,000 mV s^{-1} (c); corresponding GCD curves, operated with current densities ranging from 0.1 mA cm^{-2} to 2 mA cm^{-2}. (d).

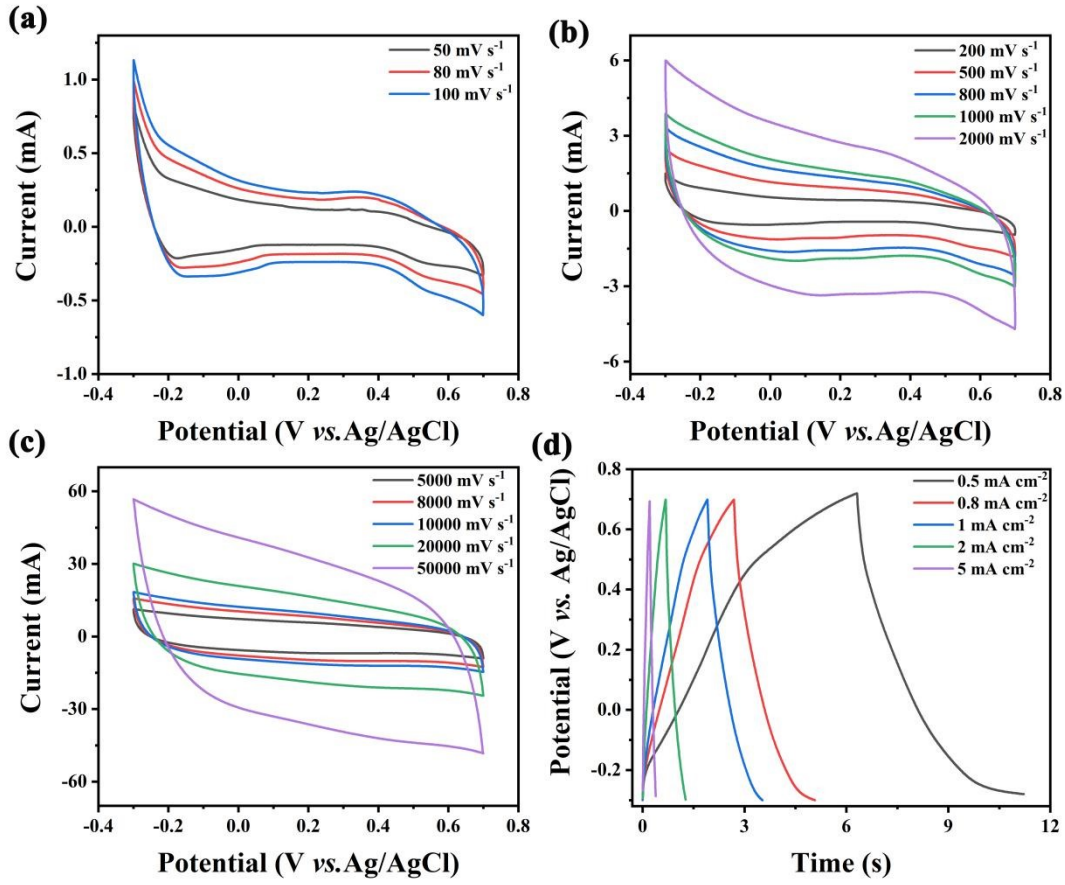

Figure S5. Three-electrode electrochemical performance of GaN-1h. CV profiles of the electrode at scan rates ranging from 50 mV s^{-1} to 100 mV s^{-1} (a); from 200 mV s^{-1} to 2,000 mV s^{-1} (b) and from 5,000 mV s^{-1} to 50,000 mV s^{-1} (c); corresponding GCD curves, operated with current densities ranging from 0.5 mA cm^{-2} to 5 mA cm^{-2} (d).

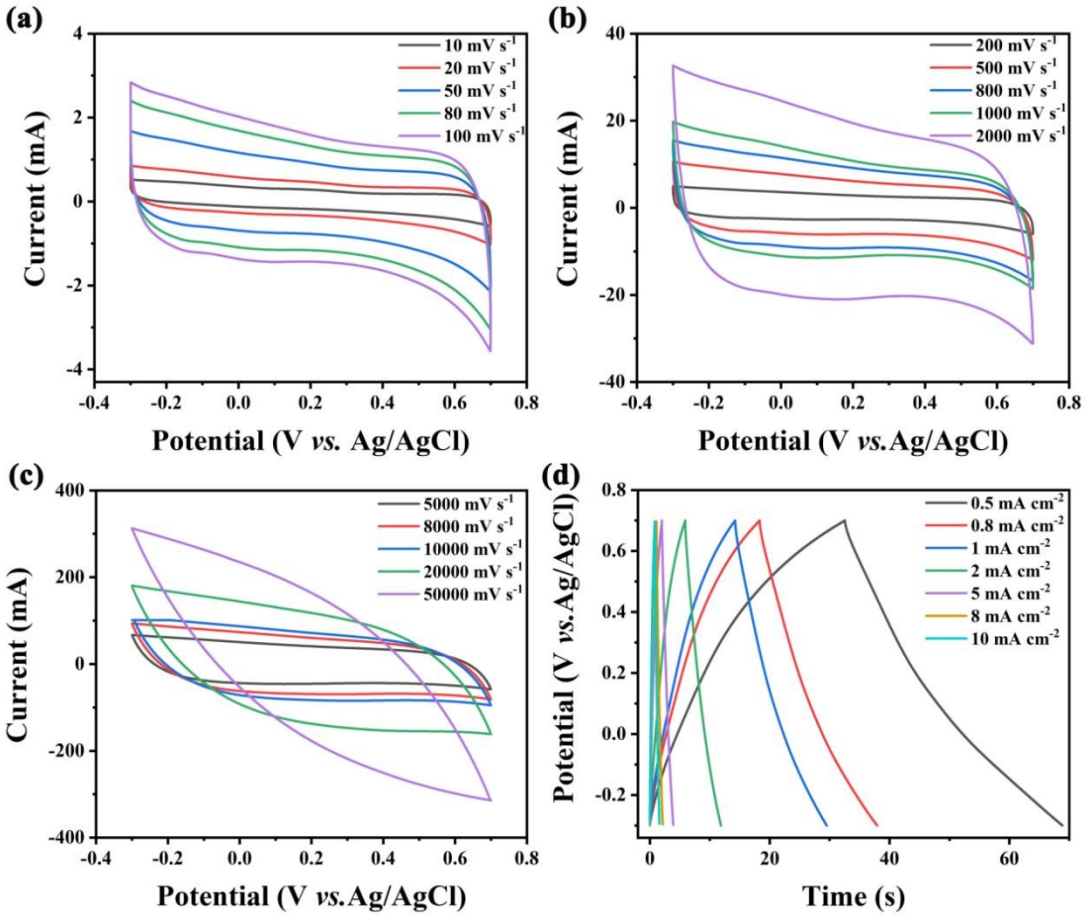

Figure S6. Three-electrode electrochemical performance of GaN-2.5h. CV profiles of the electrode at scan rates ranging from 10 mV s^{-1} to 100 mV s^{-1} (a); from 200 mV s^{-1} to 2,000 mV s^{-1} (b) and from 5,000 mV s^{-1} to 50,000 mV s^{-1} (c); corresponding GCD curves, operated with current densities ranging from 0.5 mA cm^{-2} to 10 mA cm^{-2} (d).

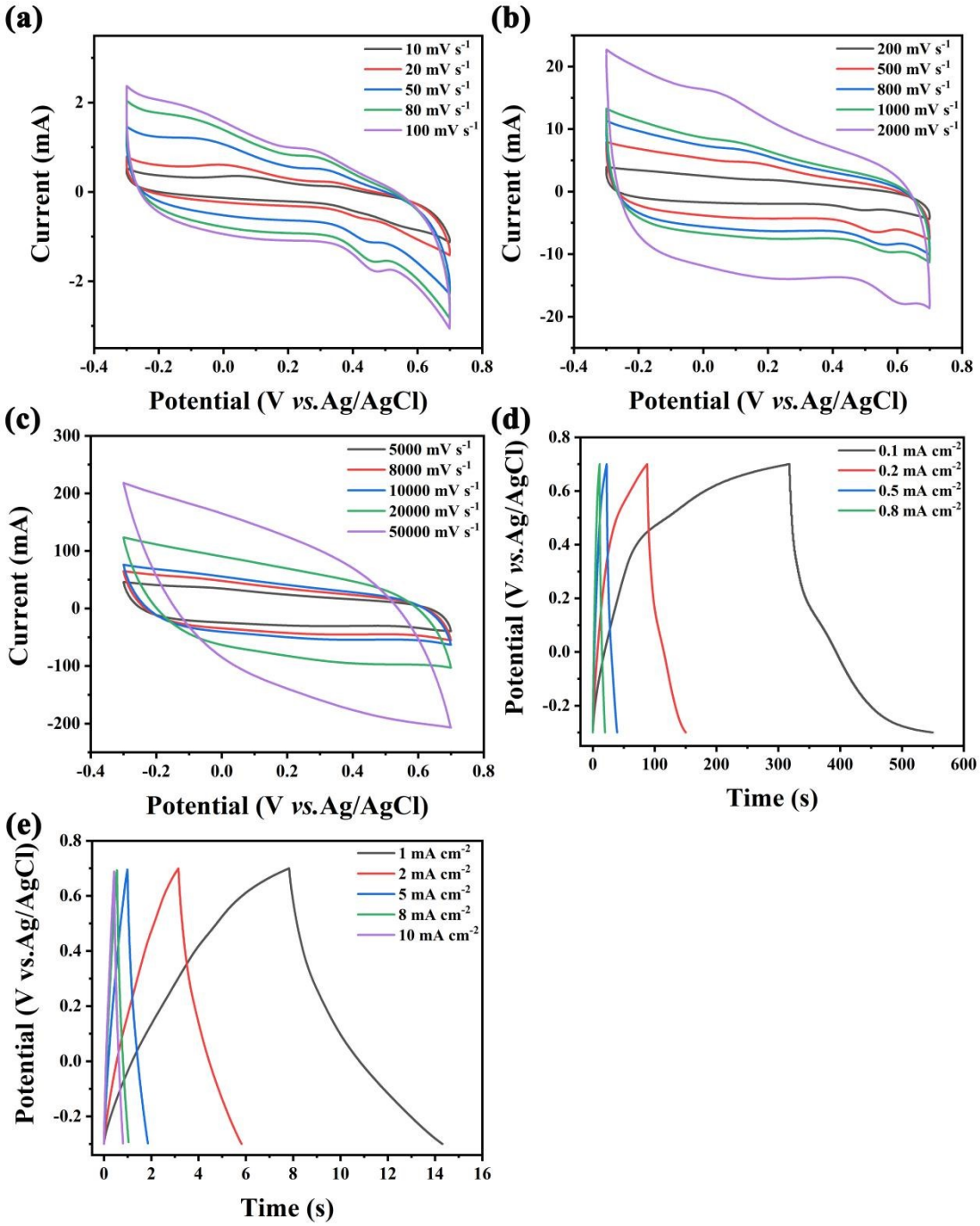

Figure S7. Three-electrode electrochemical performance of GaN-3h. CV profiles of the electrode at scan rates ranging from 10 mV s^{-1} to 100 mV s^{-1} (a); from 200 mV s^{-1} to 2,000 V s^{-1} (b); from 5,000 mV s^{-1} to 50,000 mV s^{-1} (c); corresponding GCD curves, operated with current densities ranging from 0.1 mA cm^{-2} to 0.8 mA cm^{-2} (d) and from 1 mA cm^{-2} to 10 mA cm^{-2} (e).

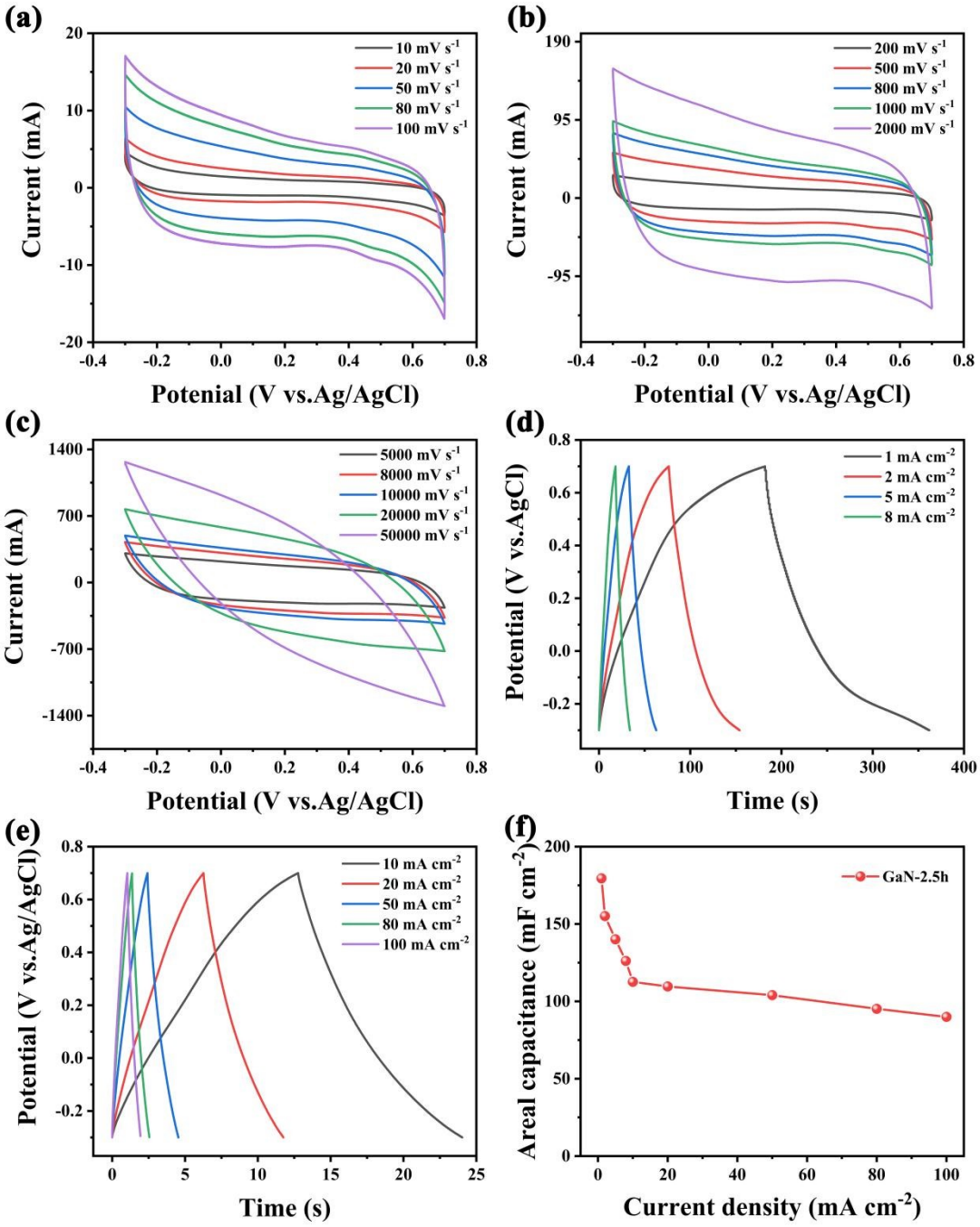

Figure S8. Three-electrode electrochemical performance of GaN-2.5h with high mass loading. CV profiles of the electrode at scan rates ranging from 10 mV s^{-1} to 100 mV s^{-1} (a); from 200 mV s^{-1} to 2,000 mV s^{-1} (b) and from 5,000 mV s^{-1} to 50,000 mV s^{-1} (c); corresponding GCD curves, operated with current densities ranging from 1 mA cm^{-2} to 8 mA cm^{-2} (d) and from 10 mA cm^{-2} to 100 mA cm^{-2}; areal capacitance as a function of current density (e).

To further meet the requirement of the industrial application, the electrochemical behaviors of the few-layered GaN-2.5h electrode with high mass loading are studied (Figure S8, Supporting Information). The initial shape of CV curves is preserved as the scan rate expanded to 50 V s^{-1}, which signifying prominent reversibility and rapid reaction kinetics. Similarly, the GCD measurements have also verified this result. It is observed that the areal capacitance retains 50% (from 179.5 mF cm^{-2} at 1 mA cm^{-2} to 90 mF cm^{-2} at 100 mA cm^{-2}) even the current density is increased by a factor of 100.

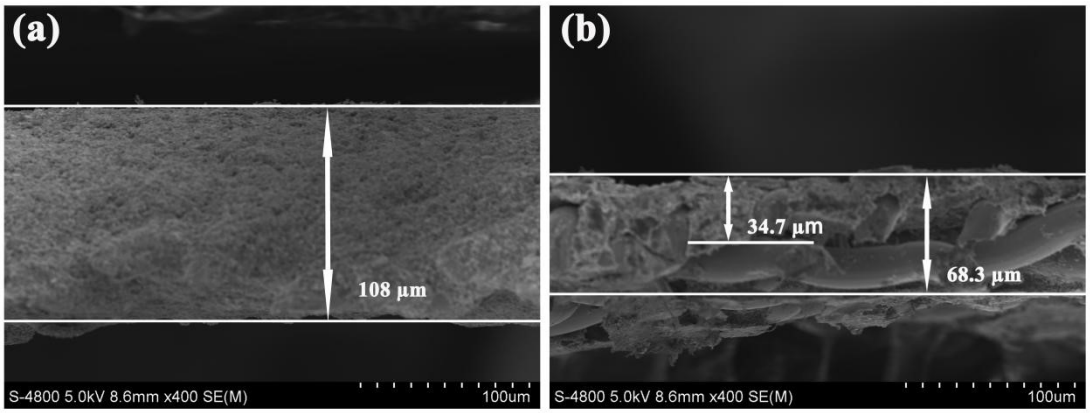

Figure S9. The cross-section SEM image of GaN-2.5h electrode film with the mass loading is approximately 6 mg cm^{-2} (a) and1 mg cm^{-2} (b), respectively.

The cross-section SEM of the electrode film suggestion that the electrode material is uniformly coated on the stainless steel mesh. It can be seen that with the increase of the mass loading, the thickness of the electrode becomes thicker.

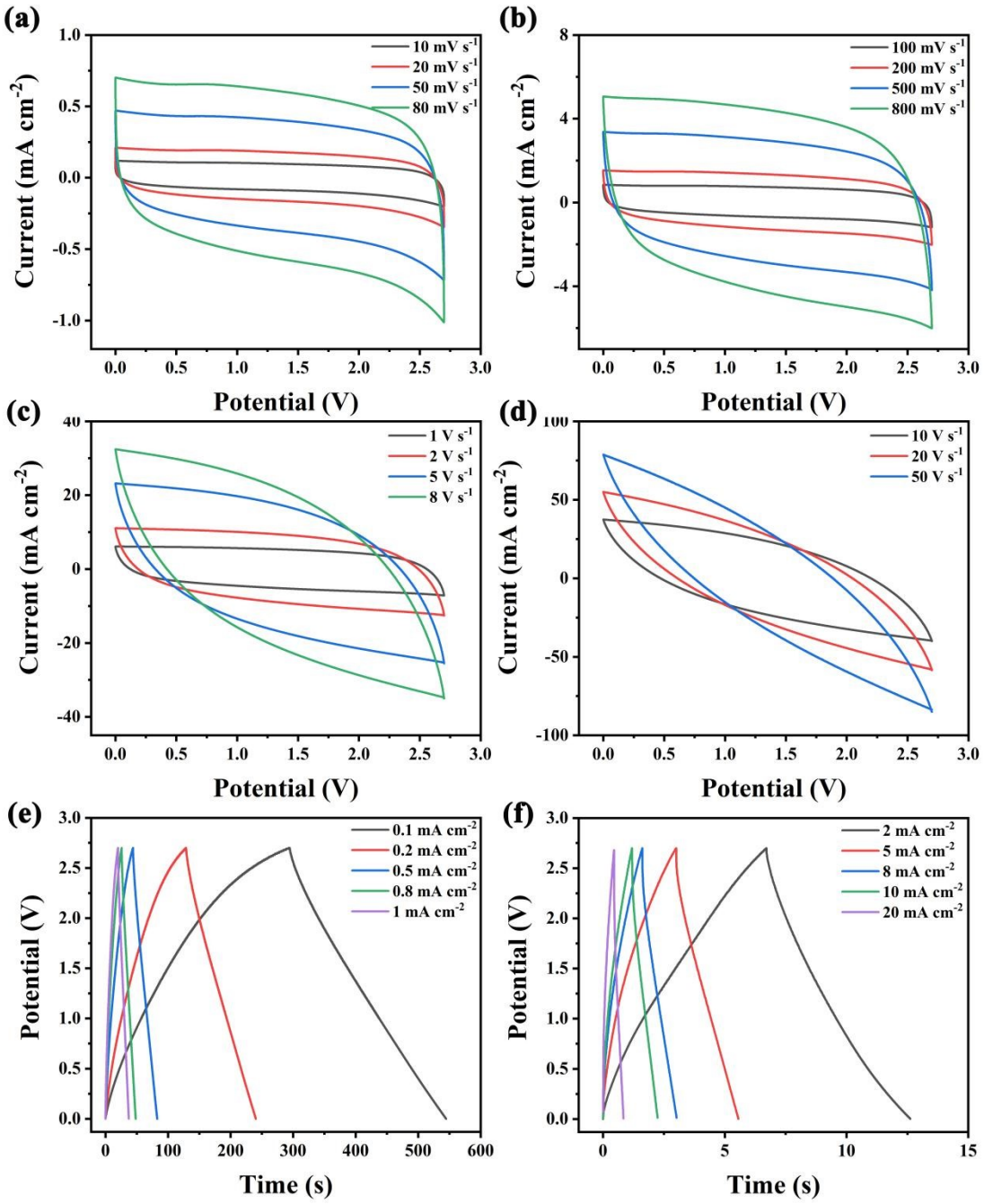

Figure S10. IL-based SC device electrochemical performance of GaN at 25 °C. CV profiles of the device at scan rates ranging from 10 mV s^{-1} to 80 mV s^{-1} (a); from 100 mV s^{-1} to 800 mV s^{-1} (b); from 1 V s^{-1} to 8 V s^{-1} (c) and from 10 V s^{-1} to 50 V s^{-1} (d); corresponding GCD curves, operated with current densities ranging from 0.1 mA cm^{-2} to 1 mA cm^{-2} (e) and from 2 mA cm^{-2} to 20 mA cm^{-2} (f).

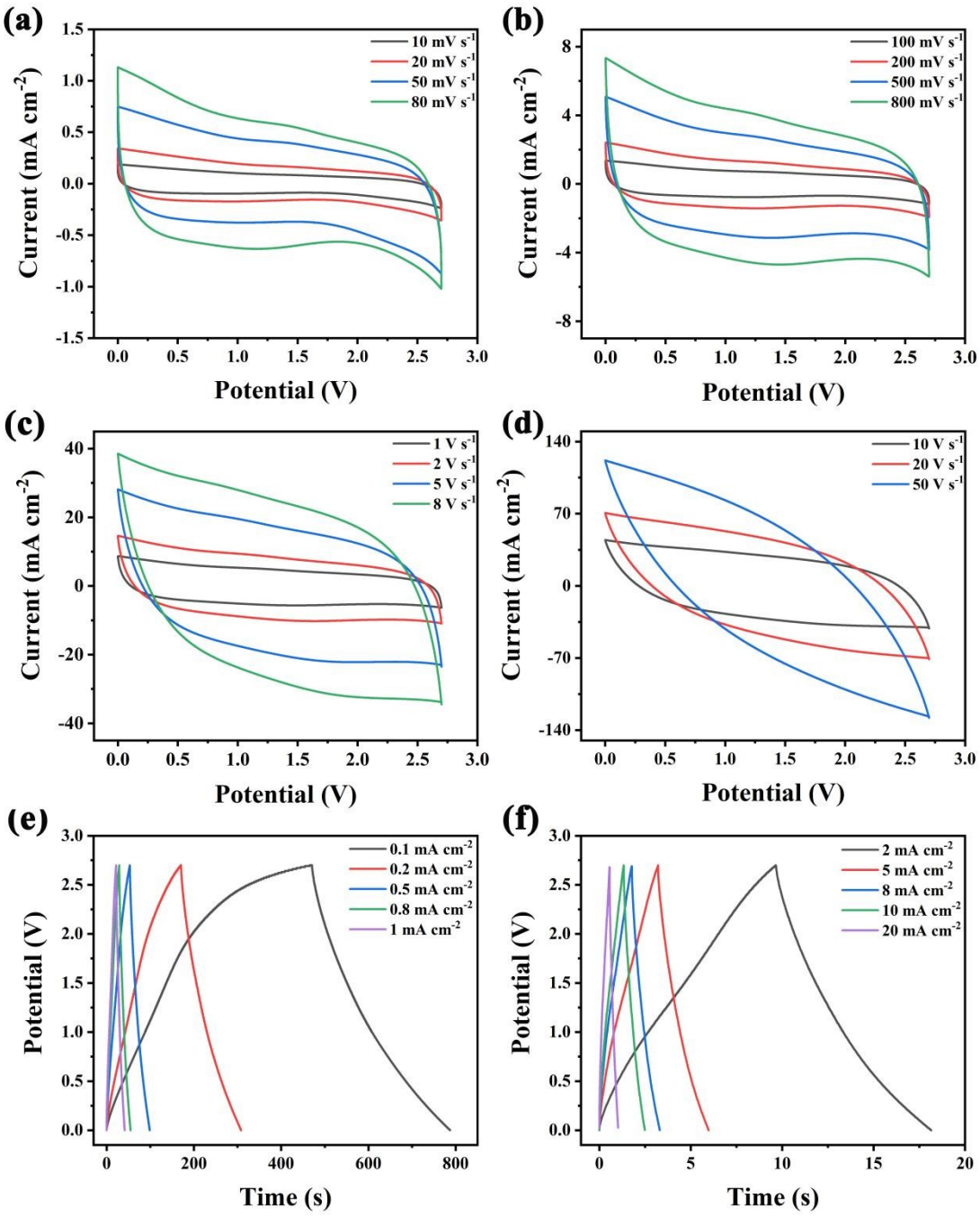

Figure S11. IL-based SC device electrochemical performance of GaN at 60 °C. CV profiles of the device at scan rates ranging from 10 mV s^{-1} to 80 mV s^{-1} (a); from 100 mV s^{-1} to 800 mV s^{-1} (b); from 1 V s^{-1} to 8 V s^{-1} (c) and from 10 V s^{-1} to 50 V s^{-1} (d); corresponding GCD curves, operated with current densities ranging from 0.1 mA cm^{-2} to 1 mA cm^{-2} (e) and from 2 mA cm^{-2} to 20 mA cm^{-2} (f).

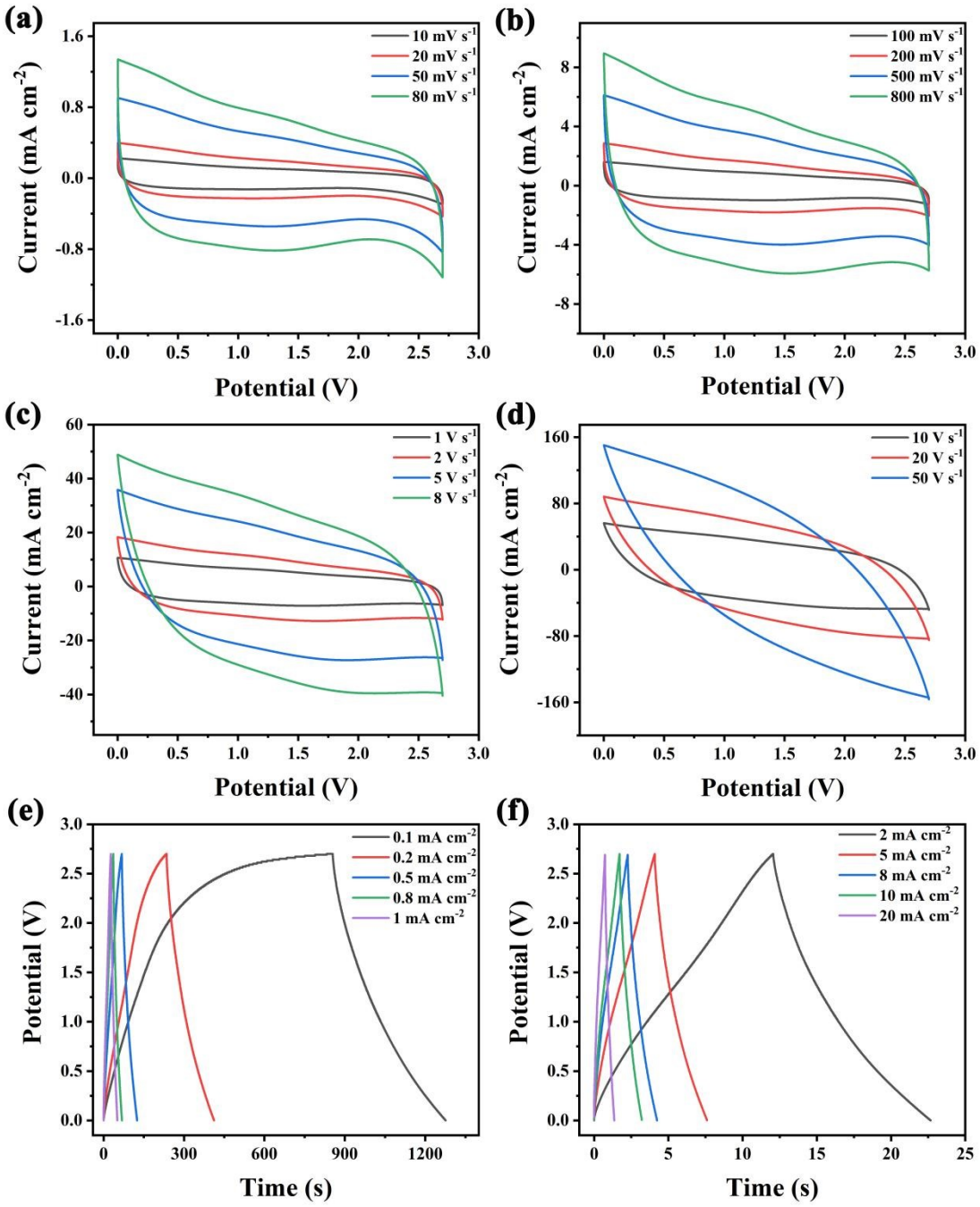

Figure S12. IL-based SC device electrochemical performance of GaN at 80 °C. CV profiles of the device at scan rates ranging from 10 mV s^{-1} to 80 mV s^{-1} (a); from 100 mV s^{-1} to 800 mV s^{-1} (b); from 1 V s^{-1} to 8 V s^{-1} (c) and from 10 V s^{-1} to 50 V s^{-1} (d); corresponding GCD curves, operated with current densities ranging from 0.1 mA cm^{-2} to 1 mA cm^{-2} (e) and from 2 mA cm^{-2} to 20 mA cm^{-2} (f).

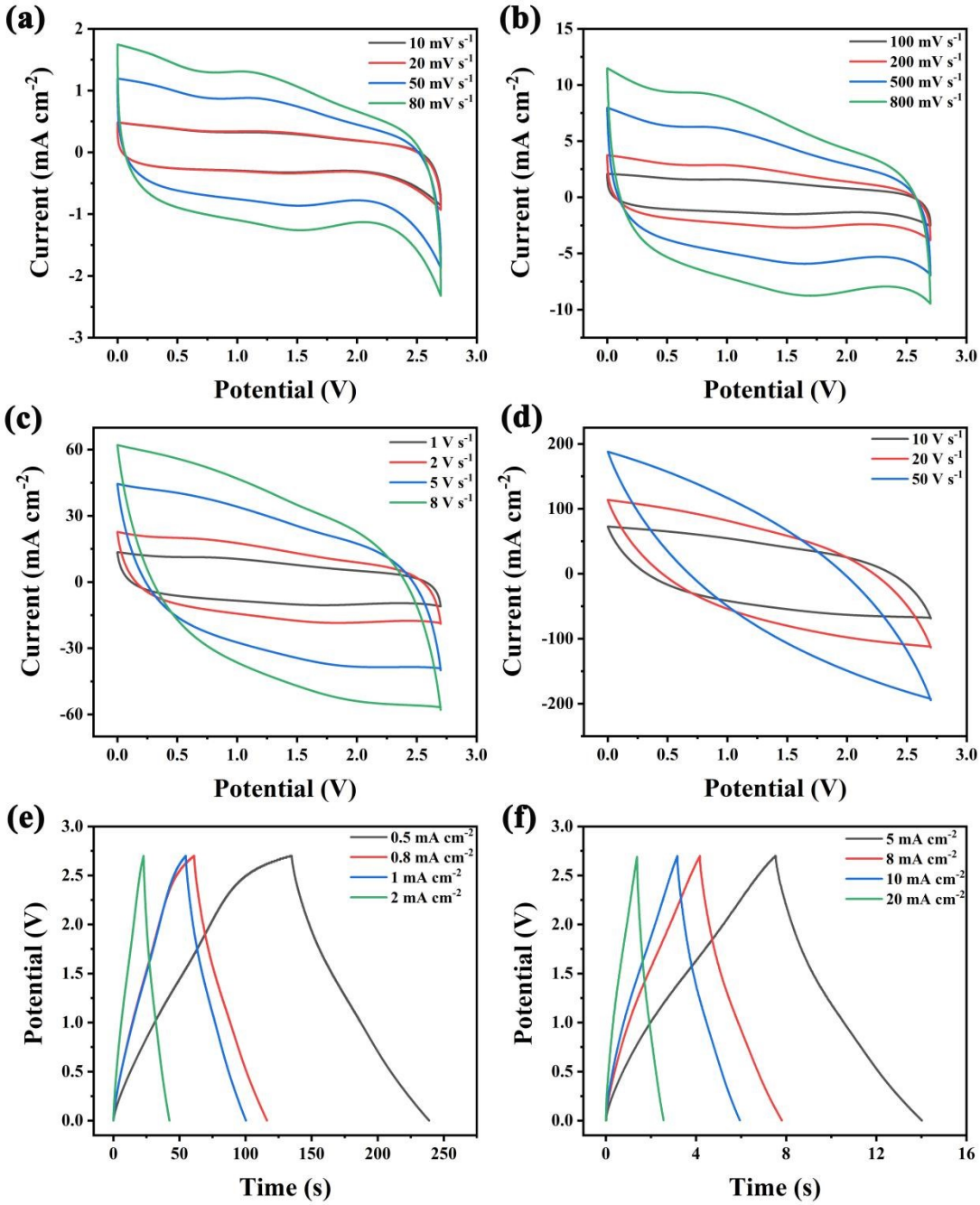

Figure S13. IL-based SC device electrochemical performance of GaN at 100 °C. CV profiles of the device at scan rates ranging from 10 mV s^{-1} to 80 mV s^{-1} (a); from 100 mV s^{-1} to 800 mV s^{-1} (b); from 1 V s^{-1} to 8 V s^{-1} (c) and from 10 V s^{-1} to 50 V s^{-1} (d); corresponding GCD curves, operated with current densities ranging from 0.5 mA cm^{-2} to 2 mA cm^{-2} (e) and from 5 mA cm^{-2} to 20 mA cm^{-2} (f).

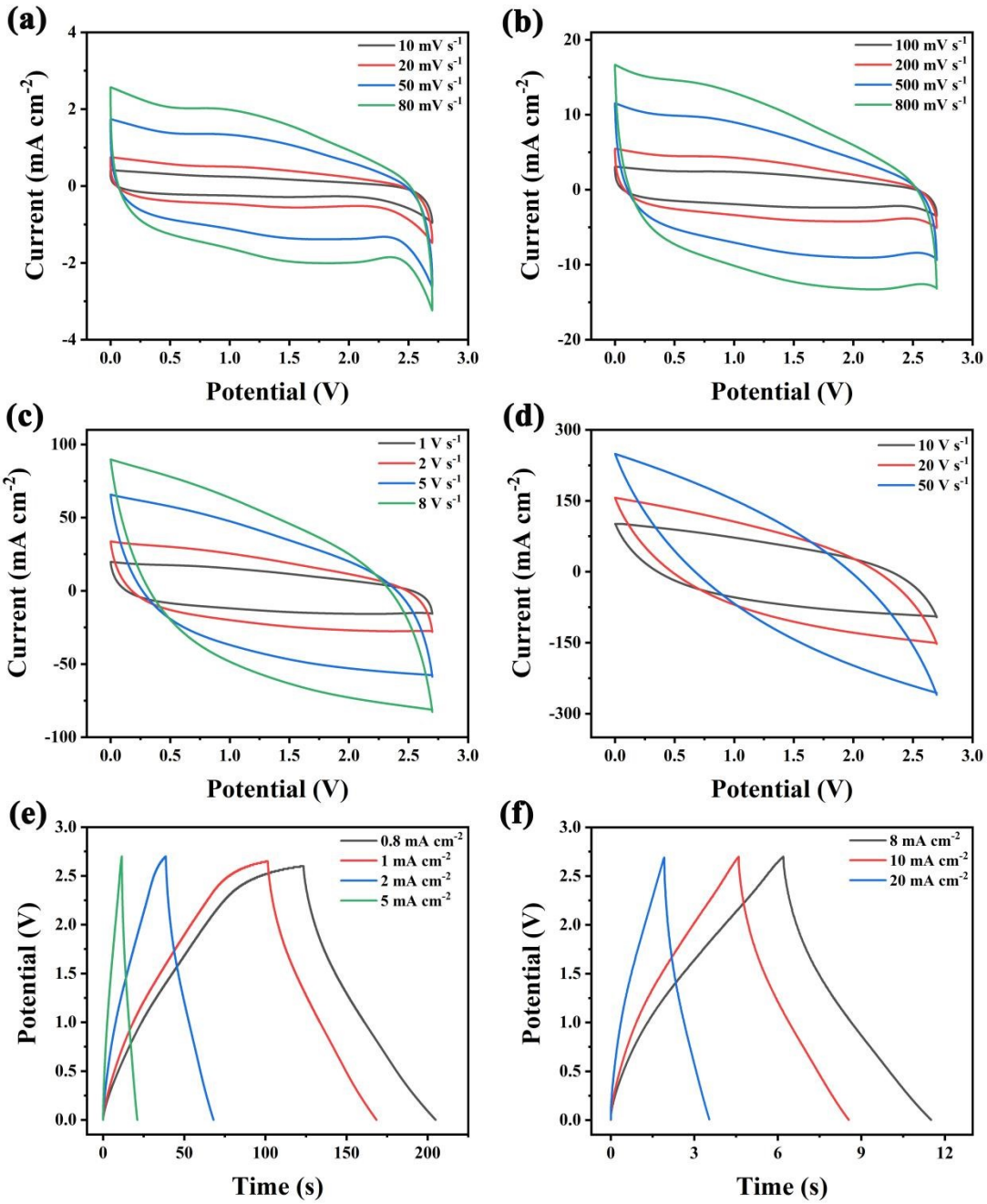

Figure S14. IL-based SC device electrochemical performance of GaN at 130 °C. CV profiles of the device at scan rates ranging from 10 mV s^{-1} to 80 mV s^{-1} (a); from 100 mV s^{-1} to 800 mV s^{-1} (b); from 1 V s^{-1} to 8 V s^{-1} (c) and from 10 V s^{-1} to 50 V s^{-1} (d); corresponding GCD curves, operated with current densities ranging from 0.8 mA cm^{-2} to 5 mA cm^{-2} (e) and from 8 mA cm^{-2} to 20 mA cm^{-2} (f).

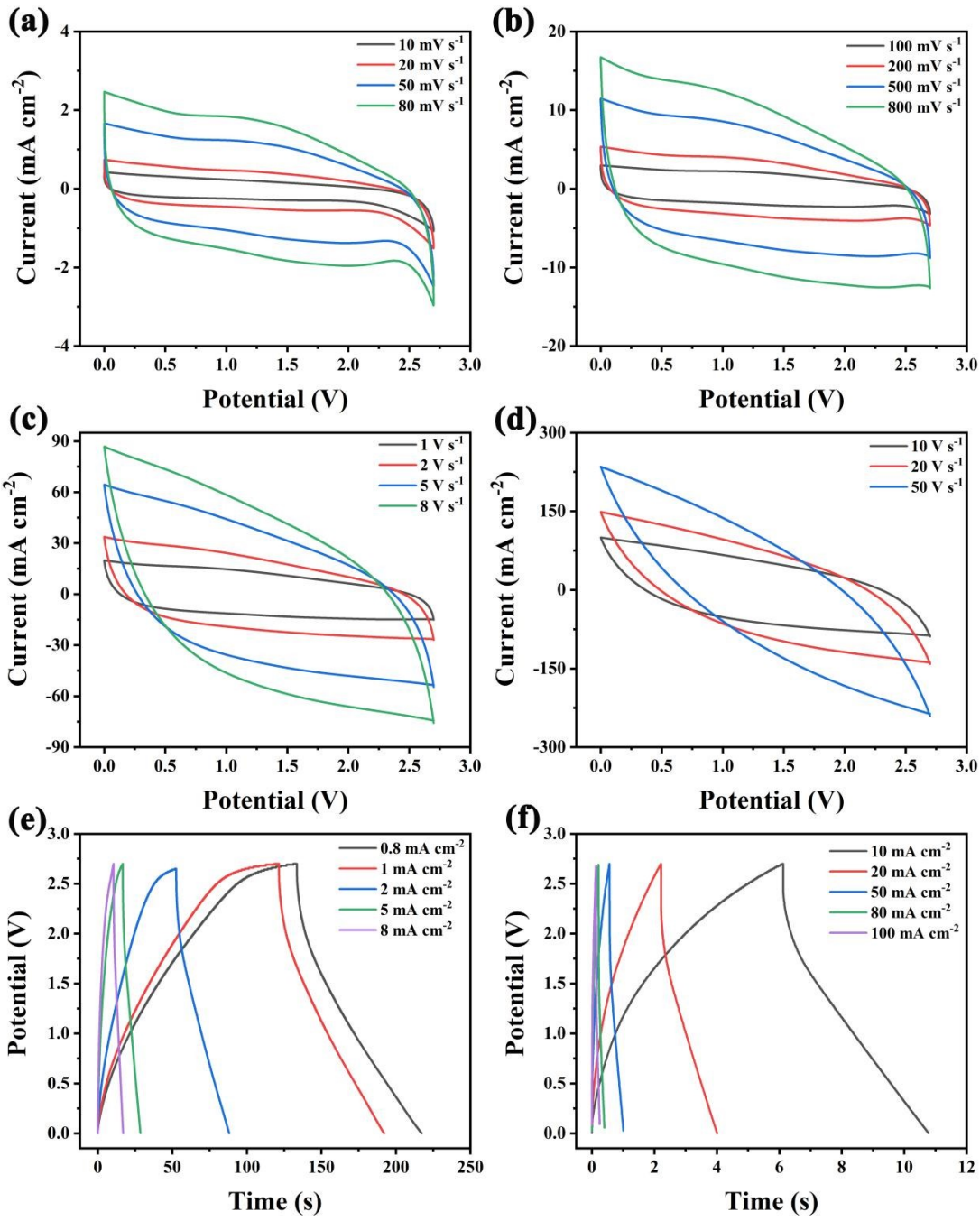

Figure S15. IL-based SC device electrochemical performance of GaN at 150 °C. CV profiles of the device at scan rates ranging from 10 mV s^{-1} to 80 mV s^{-1} (a); from 100 mV s^{-1} to 800 mV s^{-1} (b); from 1 V s^{-1} to 8 V s^{-1} (c) and from 10 V s^{-1} to 50 V s^{-1} (d); corresponding GCD curves, operated with current densities ranging from 0.8 mA cm^{-2} to 8 mA cm^{-2} (e) and from 10 mA cm^{-2} to 100 mA cm^{-2} (f).

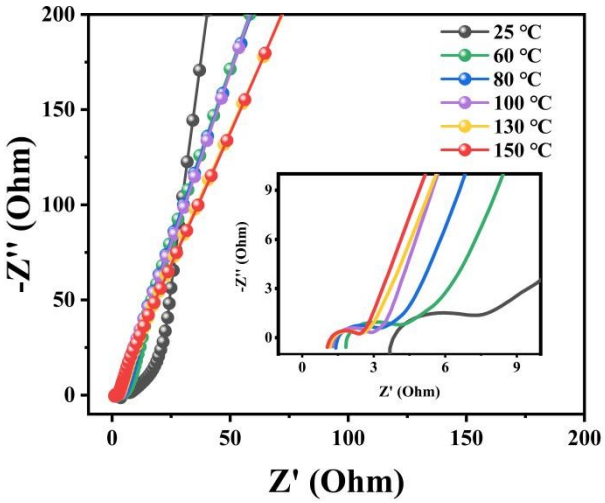

Figure S16. Few-layered GaN IL-based SC devices Nyquist plots at 25 ℃, 60 ℃, 80 ℃, 100 ℃, 130 ℃, 150 ℃.

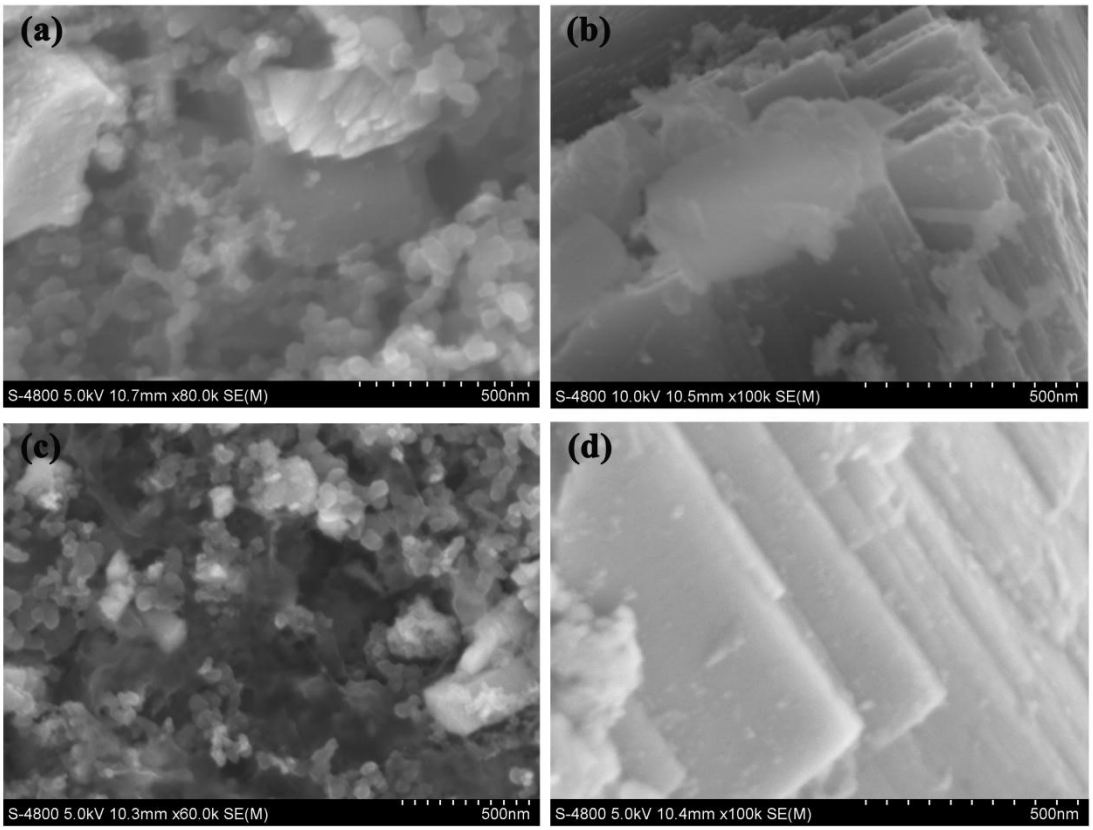

Figure S17. SEM images of the IL-based SC devices GaN electrode of 150 ℃ before (a,b) and after (c,d) 10,000 cycles at 8 mA cm^{-2}

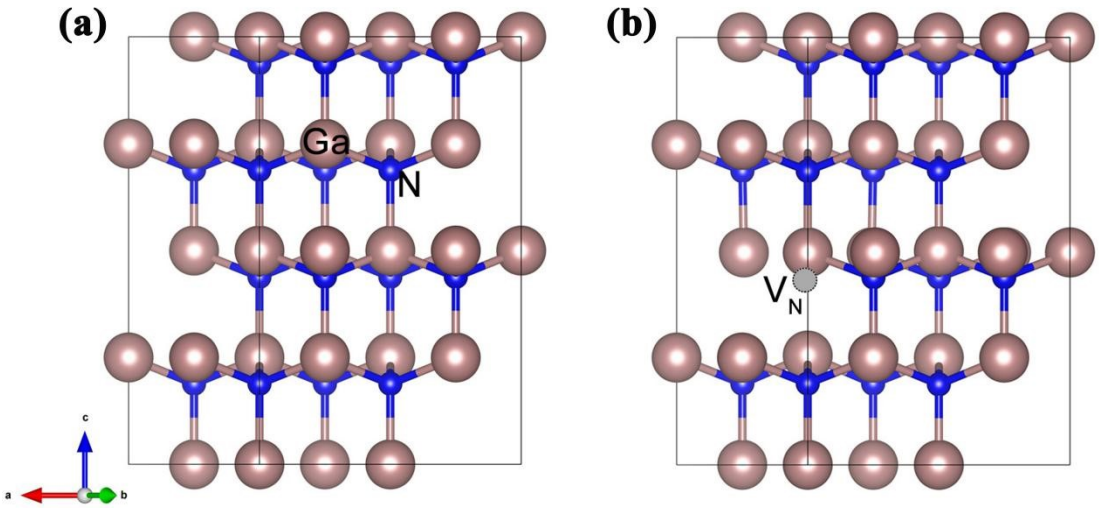

Figure S18. The optimized structures of GaN bulk (a) and the V_N@GaN bulk (b).

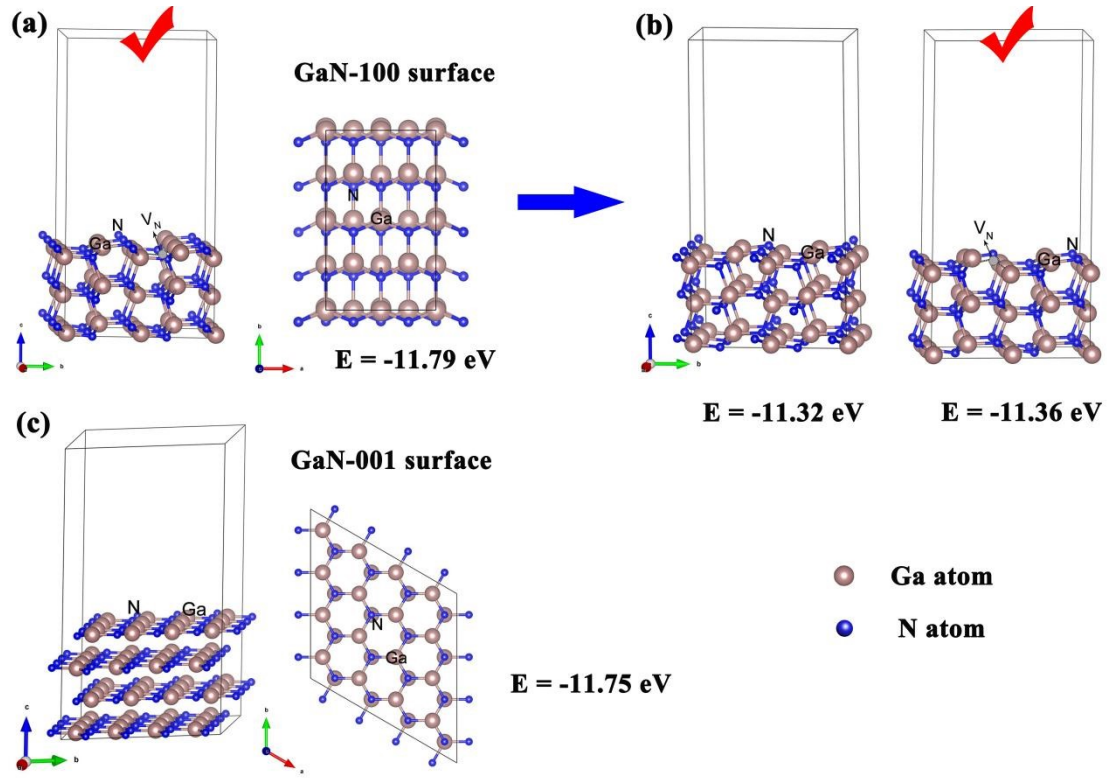

Figure S19. (a) Perfect GaN (100) surface side view (left) and top view (right); (b) the optimized structures of the V_N defects in different environments on the GaN-100 surface; (c) perfect GaN (001) surface side view (left) and top view (right).

To determine the optimal adsorption surface for $C_6H_{11}N_2$•$C_2F_6NO_4S_2$ ($EMImNFT_2$) on GaN, we first built the GaN-100 and GaN-001 surfaces in **Figure**

S19a and S19c. The thickness of vacuum spacing was ~15Å in the *z*-direction to prevent spurious interactions. Compared with GaN-001 surface (–11.75 eV), GaN-100 surface has lower energy of –11.79 eV, so we constructed a series of $EMImNFT_2$ adsorption models based on the stable GaN-100 surface. For the V_N defects on the GaN-100 surface (V_N@GaN-100 surface), the energies of V_N in different environments were –11.32 eV and –11.36 eV, respectively, as shown in **Figure S19b** left and right. Thus, a series of models for $EMImNFT_2$ adsorption, were constructed on the stable V_N@GaN-100 surface (**Figure S19b**).

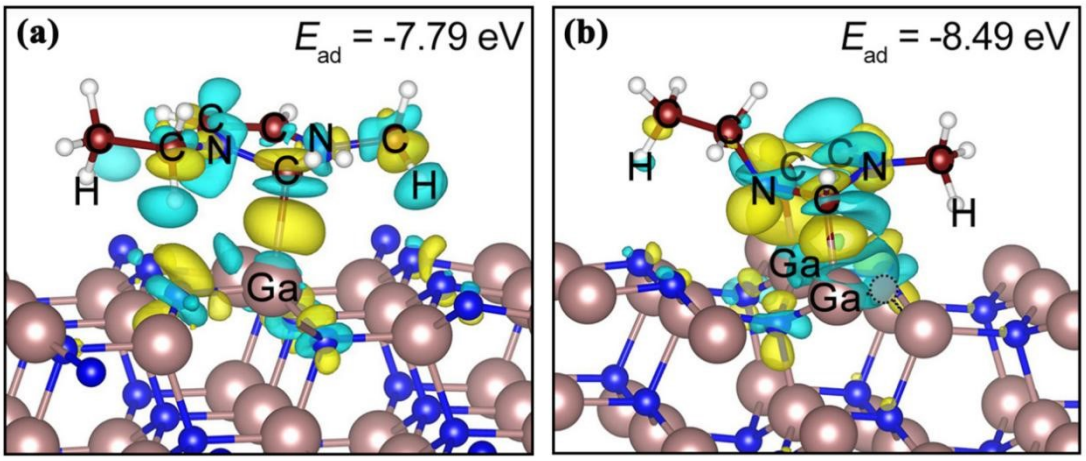

Figure S20. Calculated adsorption energies for electrolyte cation ($EMIm^+$).

Table S1. Comparison of electrochemical performance of GaN with wide-bandgap semiconductor based electrode reported in the literatures of aqueous electrolytes at 25 ℃.

Material	Specific capacitance	Stability	Ref.
GaN nanocrystalline	**34.43 mF cm^{-2} at 0.5 mA cm^{-2}**	**97.8%-10,000**	**This work**
GaN MM	23.67 mF cm^{-2} at 10 mV s^{-1}	98% - 30,000	*Adv. Mater.* **2016,** *28,* 3768
GaN PM	21.22 mF cm^{-2} at 0.1 mA cm^{-2}	99% -10,000	*Sci. Rep.* **2017,** *7,* 40063
SiC NWs arrays	23.6 mF cm^{-2} at 0.2 mA cm^{-2}	/	*Adv. Funct. Mater.* **2021,** *31,* 2008901
SiC NWs	9.56 mF cm^{-2} at 0.2 mA cm^{-1}	/	*Energy Stor. Mater.* ***2020,*** *27,* 261
SiC NWs	23.6 mF cm^{-2} at 10 mV s^{-1}	94.8%- 10,000	*Adv. Energy Mater.* **2019,** *9,* 1900073
SiC/G-HNF	0.41 mF cm^{-2} at 5 μA cm^{-2}	86% - 5,000	*Small* **2018,** *14,* 1801857
SiC nanochannels	14.8 mF cm^{-2} at 10 mV s^{-1}	96% -10,000	*Mater. Horiz.* **2018,** *5,* 883
N doped SiC NWs	4.8 mF cm^{-2} at 10 mV s^{-1}	98% -10,000	*ACS. Nano.* **2015,** *9,* 8054
SiC NWs	2.33 μF cm^{-2} at 100 mV s^{-1}	/	*ACS Appl. Mater. Interfaces* **2015,** *7,* 26658
SiC NWs	240 μF cm^{-2} at 100 mV s^{-1}	95% - 200,000	*J. Power Sources* **2013,** *230,* 298
SiC NWs array	350 μF cm^{-2} at 0.5 V s^{-1}	~100%-10,000	*Nanoscale*, **2013,** *5,* 4114
SiC NWs	23 mF cm^{-2} at 50 mV s^{-1}	90% -10,000	*J. Power Sources,* **2013,** 243, 648
SiC/C	734 μF cm^{-2} at 10 mV s^{-1}	91.2% -20,000	*J. Mater. Sci. Technol.* **2022,** *110,* 178
SiC NWs	46.7 mF cm^{-2} at 0.1 V s^{-1}	~100%-10,000	*J. Alloys Compd.* **2020,** *827,* 154168
C/PSiC	325 mF cm^{-2} at 1mA cm^{-2}	83% - 5,000	*Nano Lett.* **2014,** *14,* 1843

Table S2. Fitting report of Figure 3f insert based on a R(CR)W equivalent circuit.

index	fixed	parameter	start	end	rel. Std. error (%)
1	0	Rs	0.8562	0.8562	1.384
2	0	C	0.007263	0.007081	1.600
3	0	Rct	0.495	0.495	1.197
4	0	W	0.1649	0.1649	6.337

Table S3. Comparison of electrochemical performance of high mass loading electrode reported in the literatures.

Material	Mass loading	Max Scan rate	Capacitance retention	Ref.
GaN crystal	**~6 mg cm^{-2}**	**50 V s^{-1}**	**50% (from 1 mA cm^{-2} to 100 mA cm^{-2})**	**This work**
CNT@MnO_2	6.6 mg cm^{-2}	150 mV s^{-1}	~46% (from 1 mA cm^{-2} to 15 mA cm^{-2})	*Chem. Eng. J.*, **2019,** *368,* 525.
ZnNiCo LDH	7 mg cm^{-2}	60 mV s^{-1}	52.3% (from 3 mA cm^{-2} to 30 mA cm^{-2})	*J. Mater. Chem. A,* **2019,** *7,* 11826
NiCo LDH	5.11 mg cm^{-2}	100 mV s^{-1}	~22% (from 5 mA cm^{-2} to 30 mA cm^{-2})	*Electrochim. Acta,* **2020**, *362,* 137081
MnO_2/C	25 mg cm^{-2}	1 V s^{-1}	11% (from 0.5 mA cm^{-2} to 40 mA cm^{-2})	*Adv. Funct. Mater.*, **2021**, *31,* 2009632
WC@MnO_2	12.8 mg cm^{-2}	50 mV s^{-1}	~37.5% (from 1 mA cm^{-2} to 15 mA cm^{-2})	*Small* **2022**, *18,* 2201307
NiO/NF	17.4 mg cm^{-2}	100 mV s^{-1}	35.9% (from 2 mA cm^{-2} to 100 mA cm^{-2})	*Electrochim. Acta,* **2021**, *390,* 138772

Table S4. Comparison of electrochemical performance of GaN IL-based SC devices with others high temperature SC electrodes reported in the literatures.

Material	Temperature (°C)	Voltage window	Max Scan rate	Specific capacitance	Energy density	Power density	Capacitance retain-cycle	Ref.
GaN nanocrystalline	**150**	**0 -2.7 V**	**50 V s^{-1}**	**52.58 mF cm^{-2} at 0.8 mA cm^{-2}**	**13.3 μWh cm^{-2}**	**67.5 mW cm^{-2}**	**86.2% -10,000**	**This work**
SiC NWs arrays	150	0-2.5 V	200 mV s^{-1}	18.5 mF cm^{-2} at 2 mA cm^{-2}	/	/	80% - 10,000	*Adv. Funct. Mater.* **2021,** *31,* 2008901
Carbon cloth	120	0-1.8 V	5 mV s^{-1}	531.5 mF cm^{-2} at 4 mA cm^{-2}	283.9 μWh cm^{-2} (25 °C)	0.9 mW cm^{-2} (25 °C)	79.3% - 75	*J. Mater. Chem. A*, **2019,** *7,* 20398
SiC NWs	60	0-0.6 V	2 V s^{-1}	19.3 mF cm^{-2} at 5 mA cm^{-2}	0.64 μWh cm^{-2} (20 °C)	1.1 mW cm^{-2} (20 °C)	90% - 10,000	*J. Power Sources,* **2013,** *243,* 648
TiC fibre	65	0-1.6 V	1V s^{-1}	192 F g^{-1} at 5 A g^{-1}	15.6 Wh kg^{-1} (25 °C)	760 W kg^{-1}	85% - 50,000	*Energy Environ. Sci.,* **2015,** *8,* 1559
TiC	65	0-3 V	1 V s^{-1}	2.94 F cm^{-3} at 57.6 mA cm^{-2}	3 mWh cm^{-3}	2.9 mW cm^{-3}	98% - 75,000	*J. Mater. Chem. A,* **2016,** *4,* 18717
TiC NWs	60	0-3 V	400 V s^{-1} (25 °C)	185 F g^{-1} at 2 A g^{-1}	18.2 kWh kg^{-1}	1.6 kW kg^{-1}	96.8% - 50,000	*Small* **2017,** *13,* 1602742
Carbon	100	0-2.5 V	50 mV s^{-1}	150 mF cm^{-2} at 200 mV s^{-1}	/	/	92% - 25,000	*Energy Stor. Mater.* **2019,** *21,* 439
laser-induced graphene	100	0-2.5 V	10 mV s^{-1}	3.7 mF cm^{-2} at 10μA cm^{-2}	4.5 μWh cm^{-2}	90.5 μW cm^{-2}	75% - 3,200	*Electrochim. Acta* **2020,** *357,* 136838
FeOOH/CC	200	0-2.5 V	100 mV s^{-1}	115 mF cm^{-2} at 3 mA cm^{-2}	1.44 mWh cm^{-3}	49 mW cm^{-3}	70% - 5,000	*J. Mater. Chem. A* **2016,** *4,* 8316
GO	100	0-0.8 V	50 mV s^{-1}	96.2 mF cm^{-2} at 0.223 mA cm^{-2}	8.55 μWh cm^{-2}	0.0853 mW cm^{-2}	75.3% - 3,000	*Nano Energy* **2019,** *64* 103938
Ni foam	80	0-3.5 V	20 V s^{-1}	365 μF cm^{-2} at 1 V s^{-1}	0.05 μWh cm^{-2} (25 °C)	0.5 mW cm^{-2} (25 °C)	93.5% - 3,000 (25 °C)	*Electrochim. Acta* **2018,** *267,* 15

MnO_2//Graphene	80	0-1.4 V	100 mV s^{-1}	132 mF cm^{-2} at 2 mA cm^{-1}	50 μWh cm^{-2} (25 °C)	6.4 mW cm^{-2} (25 °C)	93% - 5,000 (25 °C)	*Nano Energy* **2017,** *38,* 127
PEDOTS-RuO_2@PEDOTS	75	0-1.5 V	50 mV s^{-1}	202.5 mF cm^{-2} at 50 mV s^{-1}	22.9 μWh cm^{-2}	/	74.3% - 2,000	*Nano Energy* **2018,** *50,* 106
commercial AC	150	0-1.5 V	100 mV s^{-1}	120 F g^{-1} at 30 mA cm^{-2}	34.8 Wh kg^{-1}	8.2 kW kg^{-1}	83% - 1,000	*Chem. Comm,* **2019,** *55,* 15081
rGO	120	-0.5-0.5V	100 mV s^{-1}	18.6 mF cm^{-2} at 50 mV s^{-1}	0.06 mWh cm^{-3}	0.9 W cm^{-3}	93% - 100,000	*ACS. Nano.* **2015,** *9,* 8069
Bio-AC	115	0-1.3 V	100 mV s^{-1}	172 F g^{-1}	7.2 Wh kg^{-1}	137.5 W kg^{-1}	63% - 100,000	*Electrochim. Acta* **2018,** *286,* 148
BCN nanotube	100	0-3 V	100 mV s^{-1}	37.6 mF cm^{-2} at 10 mA cm^{-2}	1.3 mWh cm^{-3}	24.9 mW cm^{-3}	86.1% - 200	Small, 2021, 17, 2102899
rGO	100	0-1 V	1 V s^{-1}	6.8 F cm^{-3} at 50 mV s^{-1}	0.837 mWh cm^{-3}	400 mW cm^{-3}	/	*ACS Appl. Energy Mater.* **2020,** *3,* 5693
CNT/PANI	100	0-1 V	100 mV s^{-1}	221 mF cm^{-2} at 3.33 mA cm^{-2}	/	/	93% - 5,000 (25 °C)	*J. Mater. Chem. A,* **2021,** *9,* 12051
AC	90	0-1 V	10 mV s^{-1}	272 F g^{-1} at 1 A g^{-1}	37.7 Wh kg^{-1}	678.6 W kg^{-1}	~100% -1,000	J. *Power Sources* **2018,** *379,* 60
AC	90	0-2.4 V	200 mV s^{-1}	21.93 F g^{-1} at 1 A g^{-1}	21.63 Wh kg^{-1}	1.13 kW kg^{-1}	~100% -18,000	*J. Colloid Interface Sci.* **2022,** *608,* 1162
AC	85	0-2.7 V	80 mV s^{-1}	79.1 F g^{-1} at 10 mV s^{-1}	0.03 mWh cm^{-3}	3.08 mW cm^{-3}	73% - 5,000	*J. Power Sources* **2020,** *447,* 227390
Activated Graphene	80	0-3 V	10 mV s^{-1}	28.4 mF cm^{-2} at 0.05 mA cm^{-2}	54.6 mWh cm^{-3}	4.6 W cm^{-3}	88% - 2,000	*Energy Environ. Sci.,* **2018,** *11,* 2001
La_2O_3 Nanosheet	70	0-1 V	30 mV s^{-1}	100 F g^{-1} at 30 mV s^{-1}	/	/	67% - 2,000	*Electrochim. Acta* **2018,** *260,* 449

TiC@crystalline PPy	60	–1-0.6 V	400 mV s^{-1}	326 F g^{-1} at 400 mV s^{-1}	/	/	40% - 5,000	*J. Power Sources* **2015,** *274,* 1118
AC	60	0-1.8 V	50 mV s^{-1}	262 F g^{-1}	138.6 Wh kg^{-1}	18 kW kg^{-1}	80% - 5,500	*Nano Energy* **2021,** *90,* 106500
Carbon	60	0-2.5 V	100 mV s^{-1}	182 F g^{-1} at 5 mV s^{-1}	/	/	84.9%-10,000	*Energy Stor. Mater.* **2019,** *22,* 323
SiC nanochannel	60	–0.1-0.7 V	200 mV s^{-1}	14.8 mF cm^{-2} at 10 mV s^{-1}	/	/	96.8% - 10,000	*Mater. Horiz.,* **2018,** *5,* 883
TiC	60	0-3 V	400 V s^{-1}	81.3 F cm^{-3} at 30 A g^{-1}	13.1 Wh kg^{-1}	20.2 kW kg^{-1}	96.8% - 50,000	*Small* **2017,** *13,* 1602742
MoS_2@TiO_2	60	–0.5-0.5 V	50 mV s^{-1}	60 F g^{-1} at 0.5 A g^{-1}	21 Wh kg^{-1}	1.35 kW kg^{-1}	98% - 2,000 (25 °C)	*J. Alloys Compd* **2021,** *883,* 160705
Graphene	60	0-1.5 V	500 mV s^{-1}	274 F g^{-1} at 2.4 A g^{-1}	11.5 Wh kg^{-1} (25 °C)	48.2 W kg^{-1} (25 °C)	69% - 5,000	*J. Power Sources* **2021,** *488,* 229461
AC	50	0-3V	20 mV s^{-1}	111 F g^{-1} at 0.1 A g^{-1}	9.0 Wh kg^{-1}	15.3 kW kg^{-1}	<97% - 1,000	*J. Mater. Chem. A,* **2015,** *3,* 18860
NiCo-MOF	50	0-1.8 V	100 mV s^{-1}	147.8 F g^{-1} at 1 A g^{-1}	77.7 Wh kg^{-1} (25 °C)	450 W kg^{-1} (25 °C)	92.6% - 4,000 (25 °C)	*J. Mater. Chem. A,* **2019,** *7,* 4998
Graphene Thin sheet	45	0-1 V	200 mV s^{-1}	99 F g^{-1} at 1 mA cm^{-2}	3.44 Wh kg^{-1}	99.2 kW kg^{-1}	92% - 5,000	*Nano energy* **2014,** *8,* 231

Remarks:

NWs: nanowires AC: Activated carbon rGO: Reduced graphene oxide

GO: Graphene oxide

Table S5. Comparison of the N atoms and Ga atoms band charge around the V_N active site of the perfect GaN surface and V_N@GaN.

Band Charge	N_4	N_3	Ga_4	**Ga_3**	N_2	N_1	**Ga_2**	**Ga_1**	N_6	N_5
GaN surface	–1.46	–1.47	+1.43	**+1.42**	–1.46	–1.48	**+1.51**	**+1.50**	–1.46	–1.47
V_N@GaN surface	–1.46	–1.47	+1.44	**+0.76**	–1.15		**+0.93**	**+0.78**	–1.45	–1.44

References

[1] G. Kresse, J. Furthmüller, *Phys. Rev. B,* **1996**, *54,* 11169.

[2] G. Kresse, D. Joubert, *Phys. Rev. B,* **1999,** *59,* 1758.

[3] J. P. Perdew, K. Burke, M. Ernzerhof, *Phys. Rev. Lett.,* **1996,** *77,* 3865.

[4] J. Heyd, G. E. Scuseria, M. Ernzerhof, *J. Chem. Phys.,* **2003,***118,* 8207.

[5] A. V. Krukau, O. A. Vydrov, A. F. Izmaylov, G. E. Scuseria, *J. Chem. Phys.,* **2006,** *125,* 224106.

[6] H. J. Monkhorst, J. D. Pack, *Phys Rev B,* **1976,** *13,* 5188.